Charge-Depleting Control Strategies and Fuel Optimization of Blended-Mode Plug-In Hybrid Electric Vehicles

Bingzhan Zhang, Chris Chunting Mi, *Senior Member, IEEE*, and Mengyang Zhang, *Member, IEEE*

***Abstract*—This paper investigates the fuel consumption minimization problem of a blended-mode plug-in hybrid electric vehicle (PHEV). A simplified mathematical model of the PHEV was constructed to obtain optimal solutions for depleting the battery to a given final state of charge (SOC) under constant vehicle speed. An optimal power strategy was constructed from theoretical analysis and simulation for constant speed cases and then applied to typical drive-cycle simulations for a middle-size plug-in sport utility vehicle in the Urban Dynamometer Driving Schedule, the U.S. Environmental Protection Agency US06 (Supplemental Federal Test Procedure), and the CR-City drive cycles. Simulation results indicate that the proposed control strategy is more efficient than other strategies of interest. Only the electric system loss characteristics, vehicle power demand, total battery energy, and trip distance are needed to implement the proposed control strategy in a PHEV. It does not rely on the detailed trip information other than the total trip distance. Therefore, it is possible to implement the control strategy in real time if the total trip distance is known before the trip.**

***Index Terms*—Control strategy, fuel consumption, plug-in hybrid electric vehicles (PHEVs), theoretical analysis.**

I. Introduction

PLUG-IN hybrid electric vehicles (PHEVs) use grid electricity to power the vehicle for an initial driving range, which is referred to as the charge depletion (CD) mode. Using electric energy from the utility grid to displace a part of the fuel is the major feature of PHEVs [1], [2]. There are two basic types of PHEVs: 1) extended-range electric vehicles (EREVs) and 2) blended-mode PHEVs.

EREVs offer pure electric driving capability in the initial driving range, which is called the all-electric range (AER). To realize pure electric driving in all driving conditions, EREVs are equipped with a full-sized traction motor powered by the PHEV battery pack. One of the disadvantages of the EREV is the increased system cost due to the full-sized traction motor and power requirement for the battery. The other disadvantage is the high losses in the electric system (battery and electric motor) at high power operations. These constraints have led to the concept of blended-mode PHEVs.

A blended-mode PHEV usually has less powerful electric drive capability. Therefore, it can typically achieve cruise and moderate acceleration in the electric mode at low to moderate vehicle speeds. For operations that require either higher power or higher torque, the engine must be used, either with or without electric assist, depending on the vehicle control strategy.

Control strategies for a blended-mode PHEV can be complex and multidimensional and will have significant impacts on vehicle performance, driveability, and fuel consumption [3]–[5]. One of the PHEV's primary capabilities is fuel displacement by depleting the onboard electric energy storage system (ESS) to a preset low-threshold state of charge (SOC). It is generally desirable that the onboard ESS has reached this depleted state (charge-sustaining SOC) by the end of the "designed" vehicle travel distance. On one hand, aggressive CD may result in higher electric loss incurred in the vehicle systems and adversely affect engine efficiency. On the other hand, a vehicle with less than sufficient CD operations may not achieve the fuel displacement function as designed, and the capacity of the onboard ESS is underutilized. Therefore, how we can achieve optimized CD operations in PHEV applications is one of the fundamental problems of PHEV control. It becomes more challenging in real-world applications, because the trip distance and drive scenarios are not precisely known.

Therefore, the objective of the PHEV optimization problem is to minimize the vehicle fuel consumption subject to specific constraints, e.g., component capabilities and available ESS energy. The problem can be formulated as follows:

$$\text{Objective : minimize } J = \int_0^{T_f} f(P_{eng})\,dt \tag{1}$$

$$\text{Subjected to : } \begin{cases} P_{b,\min}(t) \le P_b(t) \le P_{b,\max}(t) \\ P_{em,\min}(t) \le P_{em}(t) \le P_{em,\max}(t) \\ 0 \le P_{eng}(t) \le P_{eng,\max}(t) \\ SOC_{\min} \le SOC(t) \le SOC_{\max} \end{cases} \tag{2}$$

where P_b is the power of the battery, P_{em} is the power of the electric motor, P_{eng} is the engine power, SOC is the battery state of charge, and f is the fuel mass flow rate.

Manuscript received October 24, 2010; revised January 11, 2011 and February 24, 2011; accepted February 25, 2011. Date of publication March 3, 2011; date of current version May 16, 2011. The review of this paper was coordinated by Prof. M. E. Benbouzid.

B. Zhang was with the DTE Power Electronics Laboratory, Department of Electrical and Computer Engineering, University of Michigan–Dearborn, Dearborn, MI 48128 USA. He is now with the School of Mechanical and Automotive Engineering, Hefei University of Technology, Hefei 230009, China (e-mail: zhangbingzhan@gmail.com).

C. C. Mi is with the DTE Power Electronics Laboratory, Department of Electrical and Computer Engineering, University of Michigan–Dearborn, Dearborn, MI 48128 USA (e-mail: chrismi@umich.edu).

M. Zhang is with the Chrysler Group LLC, Auburn Hills, MI 48326 USA (e-mail: mz91@chrysler.com).

Color versions of one or more of the figures in this paper are available online at http://ieeexplore.ieee.org.

Digital Object Identifier 10.1109/TVT.2011.2122313

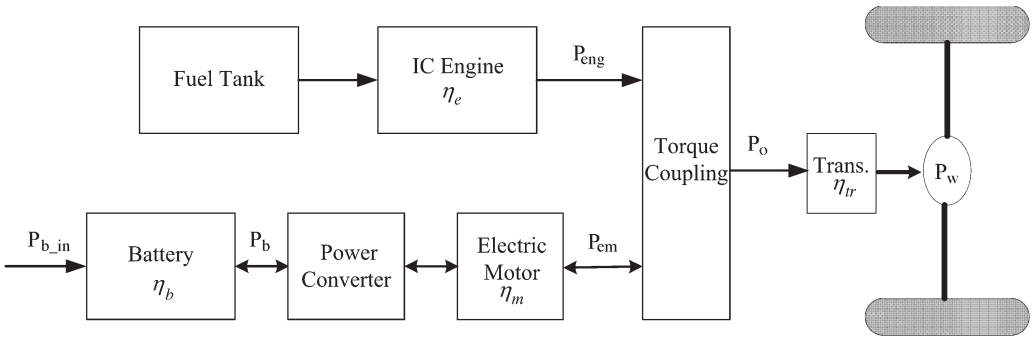

Fig. 1. Power flow of a PHEV.

TABLE I
VEHICLE PARAMETERS

Curb Weight (kg)	1988
Full Load Mass (kg)	2490
Frontal Area (m^2)	2.88
Rolling Coefficient	0.015
Wheelbase (m)	2.6
Aerodynamic Coefficient	0.41

TABLE II
HEV MAIN COMPONENTS

Fuel Converter	130 kW gasoline engine
Motor	50 kW PM Motor
Battery	360V, 24Ah lithium-ion battery

Assume that the vehicle distance traveled is greater than the AER. A fixed distance and different constant speed were used for the theoretical analysis to obtain the control parameters. The control parameters table are constructed and evaluated in the Powertrain Systems Analysis Toolkit (PSAT) with these constant-speed drive scenarios and then implemented in typical drive cycle tests.

II. VEHICLE MODEL

In this paper, a blended-mode PHEV was built in PSAT for a mid-sized plug-in sport utility vehicle (SUV). A typical parallel configuration is adopted, as shown in Fig. 1. The parallel PHEV allows both the engine and the electric motor to deliver power in parallel to drive the wheels. The propulsion power may be supplied by the engine, or the motor, or both [6]. If the motor power is sufficient, it can also realize pure electric driving mode. The electric motor can be used as a generator to charge batteries during regenerative braking or absorbing power from the engine when the engine has excessive power.

Although a generic parallel PHEV model is used for this paper, the methodology is also applicable to other types of PHEVs, including planetary-gear-based configurations, e.g., Prius and GM/Chrysler Two-Mode Hybrid, whose main operation can be considered parallel [7]–[9]. The parameters and main components of the vehicle are listed in Tables I and II.

III. ANALYSIS OF POWER FLOW IN A PLUG-IN HYBRID ELECTRIC VEHICLE

References [10] and [11] analyzed the efficiency of conventional hybrid electric vehicles (HEVs), including series and parallel HEVs. The analysis of the fuel consumption is generally operated on a specific drive cycle based on energy balance and component efficiencies. In this section, the focus is on a PHEV for specific drive cycles based on energy balance and component efficiencies.

As shown in Fig. 1, based on power balance, the power consumed to propel the vehicle P_o is equal to the power provided by the engine P_{eng} and from the electric motor P_{em}, i.e.,

$$P_o = P_{eng} + P_{em} \tag{3}$$

$$P_b = P_{em} + P_{em\_loss} \tag{4}$$

$$P_{b\_in} = P_b + P_{b\_loss} \tag{5}$$

where P_{em_loss} is the loss of the electric motor, P_{b_loss} is the loss of the battery during discharging/charging, P_b is the battery output power to the electric motor, and P_{b_in} is the battery output power, considering battery power loss. P_{em}, P_b, and P_{b_in} have signs that are positive, indicating discharging, and negative, indicating charging. P_{em_loss} and P_{b_loss} are always positive. P_o can be calculated by the following equation based on vehicle parameters and speed:

$$\frac{1}{\eta_T}\left(\frac{m_a g f_r}{3600}v + \frac{C_D A}{76140}v^3 + \frac{\delta \cdot m_a \cdot v}{3600}\frac{dv}{dt} + \frac{m_a \cdot g \cdot \sin\alpha \cdot v}{3600}\right) \tag{6}$$

where P_o is the demand power (in kilowatts), η_T is the transmission efficiency, m_a is the vehicle mass (in kilograms), g is the acceleration of gravity (in square meters per second), f_r is the rolling coefficient, v is the vehicle speed in (in kilometers per hour), C_D is the aerodynamic coefficient, A is the frontal area (in square meters), δ is the rotating mass coefficient, and α is the slope angle (in rads).

In a specific drive cycle, the total energy demand E_a and available battery energy E_b are constant, i.e.,

$$E_b = \int_0^T P_{b\_in}\, dt = const. \tag{7}$$

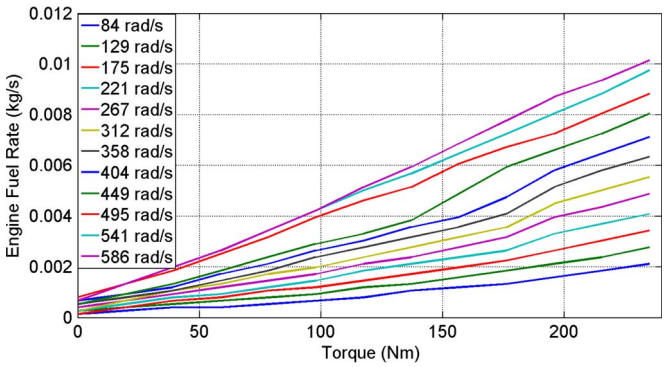

Fig. 2. Fuel rate for various engine speed.

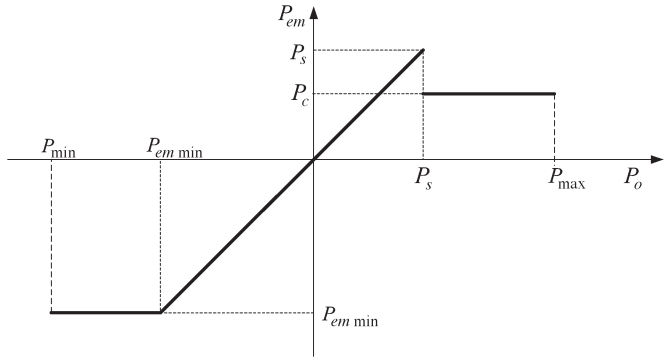

Fig. 3. Energy management strategy.

$E_b = 0$ is for charge-sustaining operations, and $E_b > 0$ is for CD operations. We have

$$E_a = \int_0^T P_o \, dt = const. \tag{8}$$

A. Fuel Consumption of an Idealized Internal Combustion Engine

The engine efficiency is represented by a nonlinear static map that describes fuel rate as a function of engine speed and engine torque, as shown in Fig. 2. It is shown that the fuel rate can approximately be represented by a linear function as engine power for each engine speed. We have

$$f\_rate = f(P_e, \omega). \tag{9}$$

For further simplicity, a linear relationship is assumed to obtain an optimized solution as

$$f = f_o + kP_{eng} \tag{10}$$

where f_o is caused by mechanical friction and pumping losses in the engine, and k approximately reflects the combustion efficiency. f_o obviously varies with different engine power ratings and increases with engine size, whereas k is almost the same for different size engines. For the specific engine used in this paper, the value of f_o and k are 1.59×10^{-1} g/s and 7.13×10^{-2} g/(kW · s), respectively.

B. Electric Power Loss

The electric losses in the PHEV include battery loss, electric motor loss, and inverter loss. These losses can be divided into the following three types: 1) the frictional and windage loss in the electric motor, which is a function of motor speed and load torque; 2) the magnetic loss in the motor, which is related to magnitude and frequency of supply voltage; and 3) copper loss in the motor and internal loss in the battery due to battery internal resistance. The last type of loss is proportional to the current squared, i.e., out power squared if the voltage is assumed to be constant. Hence, the total electric system losses include a portion that is constant (windage loss and some magnetic loss), a second portion that is proportional to the output power (a portion of frictional loss and some magnetic loss), and a third portion that is proportional to the square of output power (copper and battery losses). Therefore, we can approximate the total electric losses as a second-order polynomial as

$$P_{b\_in} = P_{em} + Loss(P_{em}) = P_{em} + L_o + AP_{em} + BP_{em}^2 \tag{11}$$

where $Loss(P_{em})$ is the electric loss, L_o, and A, B are the indices of a polynomial coefficient, which depend on vehicle powertrain components.

C. Control Strategy

The previous work has demonstrated the following three different control strategies in the CD mode [12], [13]: 1) the AER strategy; 2) the electric-dominant strategy (M1); and 3) the engine-dominant control strategy, which is also referred to as the electric assist strategy (M2). In M2, the motor size and battery power rating can be scaled down compared to the AER control strategy. If the maximum motor torque and battery power are sufficiently large, the operation is similar to the AER control strategy. The motor supplies the main driving torque, and the engine turns on when the demand toque exceeds the maximum motor torque. In M2, the engine provides most of the driving toque, and the motor assists the vehicle operation by using the onboard electric energy. The electric motor is only turned on when the road load demand exceeds the engine optimal torque/efficiency. In [14] and [15], only the engine operation is optimized, thus not using the full potential of the hybrid technology.

In this paper, as shown in Fig. 3, the proposed strategy uses electric power to drive the vehicle until a threshold power demand P_s is reached. Then, the engine turns on to meet the desired output power and electric system power with the motor to assist. A constant motor mechanical power $P_{em} = P_c$ is maintained during engine running until the end of the drive cycle. This case is referred to as the optimal power strategy (M3). We have

$$S_{eng} = \begin{cases} on, & P_o > P_s \\ off, & P_o \le P_s \end{cases} \tag{12}$$

$$P_{em} = \begin{cases} P_{em\,\min}, & P_o < P_{em\,\min} \\ P_o, & P_{em\,\min} < P_o < P_s \\ P_c, & P_s < P_o < P_{em\,\max} \end{cases} \tag{13}$$

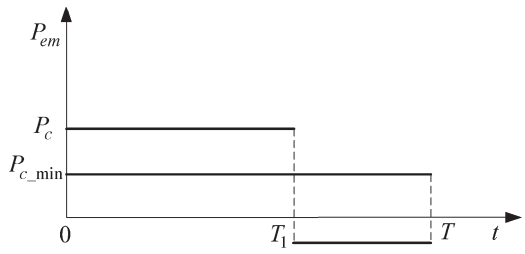

Fig. 4. Two segments in the whole trip.

where $P_{em\,\min}$ is the maximum regenerative power, and P_s is the power threshold, below which, the engine is off. P_c is the constant motor mechanical power used to assist the engine.

As shown in Fig. 4, it is assumed that, if $P_{em} = P_c$, the battery energy is used up at time T_1. If $P_{em} = P_{c\_\min}$, the battery energy is used up at time T. A fixed distance and constant speed are first used for the analysis. We have

$$T = \frac{S}{V_o} \tag{14}$$

where S is the distance, V_o is the constant speed, and T is the time of the whole trip, which depends on S and V_o. P_o is dependent on V_o.

If $P_o > P_s$, the engine will turn on, assuming that, after T_1, the battery energy will be used up. T_1 depends on P_c. During the time interval between T_1 and T, only the engine provides the energy to the vehicle. The total fuel consumption in this drive cycle is

$$\begin{aligned} m_f &= \int_0^{T_1} \dot{m}_f(P_{eng})\,dt + \int_{T_1}^{T} \dot{m}_f(P_{eng})\,dt \\ &= \int_0^{T_1} (f_o + k(P_o - P_c))\;dt + \int_{T_1}^{T} (f_o + kP_o)\,dt \\ &= (f_o + k(P_o - P_c))\,T_1 + (f_o + kP_o)(T - T_1) \\ &= (f_o + kP_o)T - kP_cT_1. \end{aligned} \tag{15}$$

According to (7) and (11), T_1 can be obtained as

$$\begin{aligned} E_b &= \int_0^{T_1} P_b\,dt = \int_0^{T_1} (Ps_c + Loss(P_c))\,dt \\ &= \left(L_o + (1+A)P_c + BP_c^2\right)T_1. \end{aligned} \tag{16}$$

Replacing T_1, (15) can be expressed as

$$m_f = (f_o + kP_o)T - \frac{kE_bP_c}{L_o + (1+A)P_c + BP_c^2}. \tag{17}$$

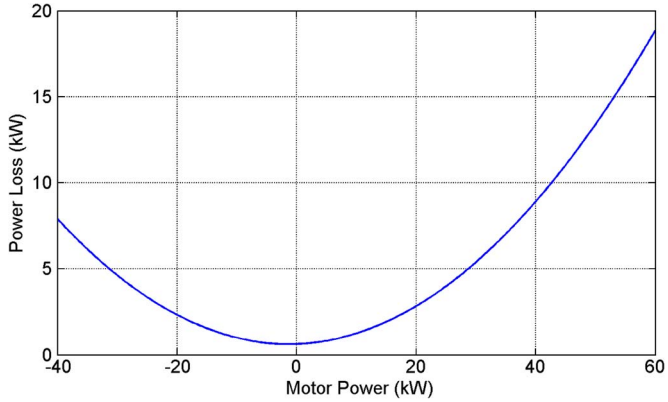

Fig. 5. Electric power loss characteristics.

By calculating the derivative of (17), the following equation can be obtained:

$$\begin{aligned} \frac{dm_f}{dP_c} &= -kE_b \frac{\left(L_o + (1+A)P_c + BP_c^2\right) - P_c(1 + A + 2BP_c)}{\left(L_o + (1+A)P_c + BP_c^2\right)^2} \\ &= -kE_b \frac{L_o - BP_c^2}{\left(L_o + (1+A)P_c + BP_c^2\right)^2}. \end{aligned} \tag{18}$$

Setting (18) to zero and solving for P_c, the solution can be obtained as

$$P_c = \sqrt{\frac{L_o}{B}}. \tag{19}$$

By calculating the second derivative of (15), (20), shown at the bottom of the page, can be obtained. Replacing $BP_c^2 = L_o$, the following equation can be derived:

$$\frac{d^2m_f}{d^2P_c} = \frac{2kE_bL_o\left(2\sqrt{BL_o} + 1 + A\right)}{\left(L_o + (1+A)P_c + BP_c^2\right)^3} > 0. \tag{21}$$

Hence, $P_c = \sqrt{L_o/B}$ is a minimal of (17). It means that, if the engine is on, the best fuel economy can be obtained when $P_c = \sqrt{L_o/B}$. This value depends on the loss characteristics of the electric system L_o and B.

If $T_1 = T$, based on (16), we can get the motor minimum power $P_{\min}$ to ensure that the battery can be used up. That is, the battery SOC drops to a preset low threshold at the end of the trip. We have

$$P_{c\_\min} = \frac{-(1+A) + \sqrt{(1+A)^2 - 4B\left(L_o - \frac{E_b}{T}\right)}}{2B}. \tag{22}$$

Considering the ideal condition, if the power loss is zero, i.e., $L_o \to 0$, $A \to 0$, $B \to 0$, and $\lim P_{c\_\min} = E_b/T$. This condition is also consistent with the assumption. Based on the relationship among P_o, $\sqrt{L_o/B}$, and $P_{c\_\min}$ and

$$\frac{d^2m_f}{d^2P_c} = \frac{2kE_b\left(-2B^2P_c^4 + B^2P_c^3 + 2L_oBP_c^2 + BL_oP_c + L_o + L_oA\right)}{\left(L_o + (1+A)P_c + BP_c^2\right)^3} \tag{20}$$

TABLE III
CALCULATION RESULTS (FOR A TOTAL DRIVING RANGE OF 40 mi)

Vehicle Speed	Power demand (kW)	Pmin (kW)	M 1	M 2		M 3	
			(kg)	(kg)	(%)	(kg)	(%)
30mph	6.15	3.77	1.13	1.69	49.50	/	/
40mph	10.53	5.20	1.79	2.13	19.14	/	/
50mph	16.77	6.62	2.64	2.83	7.41	2.81	6.47
60mph	25.32	8.01	3.68	3.76	2.15	3.75	1.86
67mph	32.83	8.98	4.51	4.51	0	4.51	0
70mph	36.58	9.39	4.90	4.87	-0.54	4.86	-0.61
80mph	51.00	10.75	6.35	6.17	-2.80	6.17	-2.80
90mph	69.00	12.1	7.83	7.65	-2.27	7.72	-1.39
100mph	90.95	13.43	9.48	9.30	-1.86	9.52	+0.44

In the table above, M1: electric dominant control strategy; M2: electric assist control strategy; M3: optimal power strategy.

considering (18) and (21), the results can be discussed as follows.

1) If $P_o < \sqrt{L_o/B}$, then $dm_f/dP_c < 0$, and the fuel consumption decreases with the increase of P_c.
2) If $P_{c\_\min} \le \sqrt{L_o/B} \le P_o$, the fuel consumption has a minimum value at $P_c = \sqrt{L_o/B}$.
3) If $P_{c\_\min} > \sqrt{L_o/B}$, then $dm_f/dP_c > 0$, and the fuel consumption increases with P_c.

If $P_c = P_o$, from 0 to T_1, the engine will be turned off, which means that the vehicle is in the AER mode. The total fuel consumption becomes

$$m_f = \int_{T_1}^{T} \dot{m}_f(P_{eng})\,dt = \int_{T_1}^{T} f_o + kP_o\,dt = (f_o + kP_o)(T - T_1). \tag{23}$$

The aforementioned set points for P_c can be used for the control of PHEV to optimize fuel economy (minimize fuel consumption). Based on the aforementioned analysis, it seems that, because the optimal values of P_c depend on P_o, $P_{c\_\min}$, and $\sqrt{L_o/B}$, we will need to calculate their values based on the drive cycle and then decide on the engine turn-on threshold, as well as the battery/motor power once the engine has been turned on. Hence, the control can be described in the following steps.

- Obtain L_o, B, and A for the electric systems. This approach can be done based on the simulations of the electric system or through experiments of the actual electric system, including the battery, inverter, and electric motor.
- Calculate $\sqrt{L_o/B}$ and $P_{c\_\min}$.
- In drive cycle simulations or real-world driving, calculate the power demand of the vehicle P_o. The power demand is determined by looking at the pedal positions and the auxiliary electric power demand.

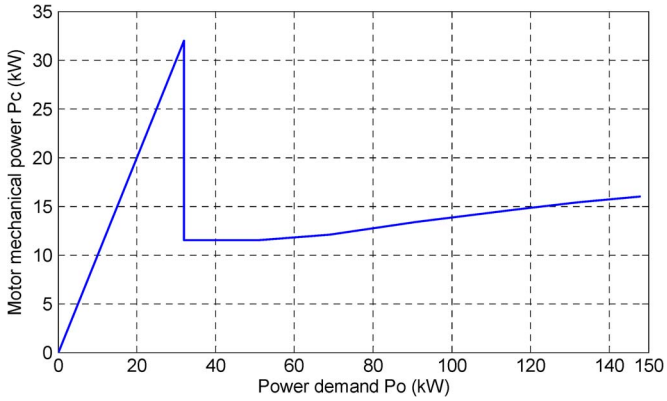

Fig. 6. Optimal motor mechanical power with different vehicle power demands.

- If $P_o \le \sqrt{L_o/B}$, then run the vehicle in the pure electric mode. The engine is off.
- If $P_o > \sqrt{L_o/B}$ but $\sqrt{L_o/B} \ge P_{C\_\min}$, then turn the engine on. Setting the motor to provide constant power of $P_c = \sqrt{L_o/B}$, the engine should provide the difference between power demand and motor power, i.e., $P_{engine} = P_o - \sqrt{L_o/B}$.
- If $\sqrt{L_o/B} \le P_{C\_\min}$, then also turn the engine on. Setting the motor to provide constant power of $P_c = P_{c\_\min}$, the engine should provide the difference between power demand and motor power, i.e., $P_{engine} = P_o - P_{c\_\min}$.

It is shown that the engine turn-on threshold and motor power are only determined by the power demand, the electric system loss characteristics, and the total battery energy. The control strategy is based on the optimal power of each component and the vehicle power demand. Hence, it is referred to as M3 in this paper. The control can easily be implemented in a vehicle controller.

TABLE IV
CONSTANT-SPEED-CYCLE SIMULATION RESULTS

Vehicle Speed	Fuel consumption (kg) (AER)		Fuel consumption (kg) (Proposed optimal power strategy)	Fuel savings (%) comparison to results from PSAT
	Analytical	PSAT	PSAT	
30mph	1.13	1.45	1.45	0
40mph	1.79	1.84	1.84	0
50mph	2.64	2.66	2.66	0
60mph	3.68	3.61	3.60	0.28
70mph	4.90	4.82	4.76	1.25
80mph	6.35	6.11	6.04	1.15
90mph	7.83	7.85	7.54	3.95

IV. CONSTRUCTION OF THE PARAMETER TABLE

In this section, we will use constant driving profiles to obtain the control parameter table, which can be used for transient drive cycles. First, the electric system loss can be obtained using experimental data. The data were used to fit a second-order curve to obtain L_o, A, and B, as shown in Fig. 5, where $L_o = 0.649$, $A = 1.23 \times 10^{-2}$, and $B = 4.85 \times 10^{-3}$. According to (19), $P_{c\_opt} = \sqrt{L_o/B} = 11.5$ kW. To calculate the fuel consumption using the equations derived in Section III, a target CD range of 40 mi is selected.

Three different control strategies were studied, as described in Section III: 1) M1; 2) M2; and M3. In mode 2, $P_{c\_\min}$ can be calculated from the vehicle parameters and the known constant speed, and we can ensure that $P_c = P_{c\_\min}$. This case means that the available battery energy is just exhausted at the end of the trip. Because $P_{\min}$ needs to first be obtained, it is difficult to implement in real-time simulations, unless the trip distance is known. However, it can be used as a theoretical calculation to construct the control parameter table. Mode 3 works only when $P_o > P_{c\_opt}$, $P_c = P_{c\_opt}$ at this time.

The fuel consumption is calculated based on the aforementioned analysis, and the results are listed in Table III. As shown in Table III, when the vehicle speeds are set at 30 and 40 mi/h, the total power demand is less than the optimal power P_{c_opt}. Therefore, the vehicle operates in mode 1, and $P_c = P_o$. The AER-mode control strategy has the best fuel economy.

When the vehicle speed is set at 50, 60, and 67 mi/h and if the engine is on, mode 2, i.e., $P_c = \sqrt{L_o/B}$ is better. However, the AER-mode control strategy is still the best in this scenario.

When the vehicle speed is set at 70 and 80 mi/h, mode 3 has the best performance among all the three control strategies. Through the aforementioned results, the engine off threshold can be obtained.

When the vehicle speed is set at 90 and 100 mi/h, the total power demand is greater than the motor maximum power, and the engine has to be turned on all the time. At this time, $P_c = P_{\min}$, mode 2 has the best fuel economy.

Based on Table III, the engine on/off threshold was 32 kW. The optimal motor mechanical power with different vehicle power demands was obtained and described as a curve, as shown in Fig. 6. The table data can be used to implement vehicle control strategies in the simulation model.

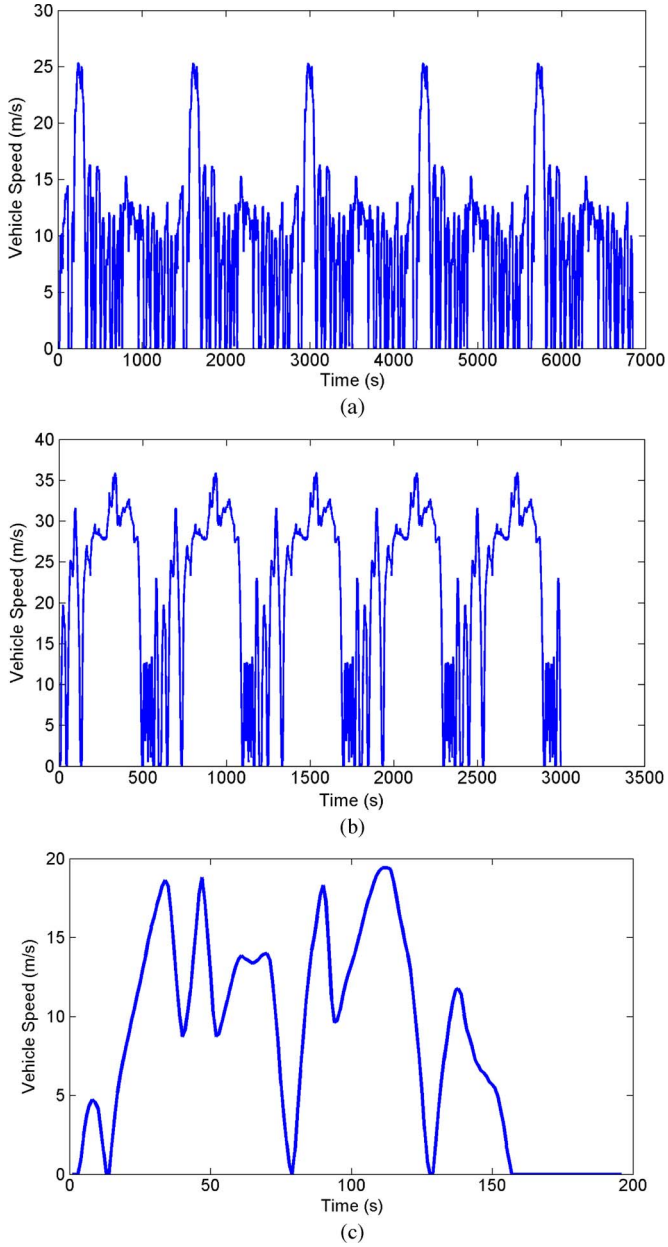

Fig. 7. Three typical drive cycles for the verification of the proposed optimal power control strategy. (a). Five consecutive UDDS drive cycles. (b). Five consecutive US06 drive cycles. (c). CR-City drive cycle.

TABLE V
COMPARISON OF THE THREE DRIVE CYCLES

	Maximum Speed (mph)	Average Speed (mph)	Maximum Acceleration (m/s^2)	Maximum Deceleration (m/s^2)	Cycle Trip Distance (miles)	Total # of Cycles
UDDS	56.7	19.6	1.48	-1.48	7.45	5
US06	80.3	50.0	3.76	-3.10	8.01	5
CR City	43.4	18.4	2.60	-3.31	1.00	40

V. SIMULATION RESULTS

First, we use PSAT to simulate the vehicle fuel economy in constant drive cycles to gain the confidence of the proposed strategy. Table IV shows the simulated results from PSAT for the different constant speed driving profiles for the proposed M3 and the default AED strategies. For ease of comparison, in the same table, we have also listed the fuel economy of the AED strategy calculated using the analytical method from the previous section. Table IV shows the following two observations: 1) The simulated fuel economy is very close to the calculated fuel economy shown in Table III, and hence, it validates the equations and parameters derived in the previous section; and 2) there is no improvement in 30, 40, 50, and 60 mi/h by using the proposed M3, because the power demand is less than the threshold for the engine to turn on. As the power demand increases, the proposed M3 shows fuel savings in 70, 80, and 90 mi/h.

This simple simulation shows that the proposed control strategy can help save fuel consumption as the power demand increases. Because power demand in transient drive cycles is much higher, the estimated fuel savings can be more significant. Hence, it is important to see how well the proposed strategy performs in various transient drive cycles. For this purpose, the proposed strategy is applied to the Urban Dynamometer Driving Schedule (UDDS), the U.S. Environmental Protection Agency US06 (Supplemental Federal Test Procedure), and the CR-City drive cycles, as shown in Fig. 7.

Compared to UDDS, the US06 and CR-City drive cycles are more aggressive in terms of acceleration and deceleration, which better approximate aggressive driving in the real world. A comparison among the three cycles is shown in Table V.

The electric range was also tested in the UDDS drive cycle. The SUV can run 23 mi in the electric range until the battery SOC drops to 0.3, as shown in Fig. 8. The results indicate that the battery parameters selected for the SUV are appropriate.

For fuel economy comparison, the battery final SOC must be at the same level; therefore, SOC correction is necessary. In [18] and [19], the linear regression method was used to ensure that the initial and final SOCs are the same. In this paper, the initial SOC value is 1.0, and the target SOC value is 0.3; therefore, the difference between the final SOC and the target value is considered. Linear fitting was adopted to determine the fuel consumption by setting the difference value to zero. Fig. 9 shows an example of SOC correction for fuel consumption in a random drive cycle.

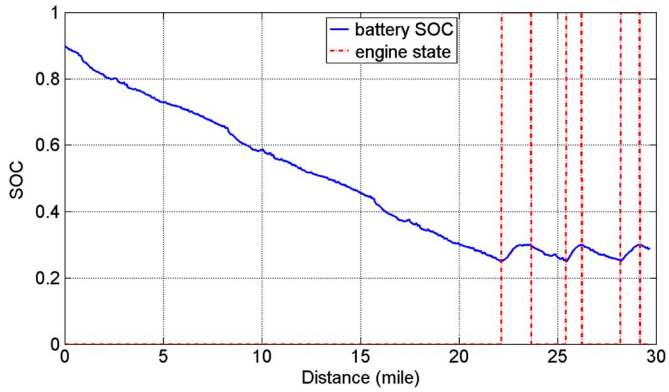

Fig. 8. Electric range in UDDS.

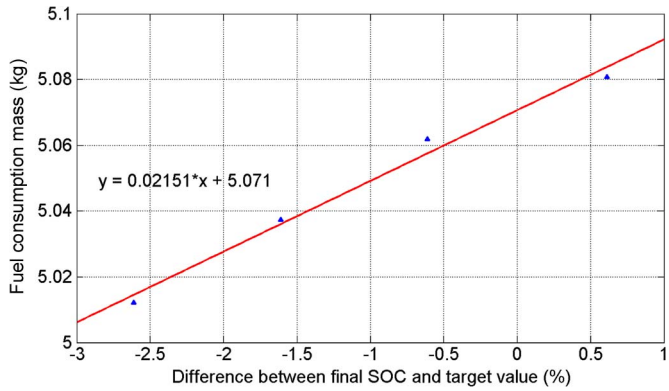

Fig. 9. Example of SOC correction in a random drive cycle.

The different drive cycles are simulated in PSAT by incorporating the proposed optimal power control strategies. Fig. 10 shows the power demand of the different drive cycles. The power distribution between the engine and the motor are determined by the proposed control strategy M3. Fig. 11 shows the power distribution between the engine and the motor for the CR-City drive cycle. It is shown that the power distribution between the engine and the motor follows the proposed control strategy M3. When the power demand is less than the optimal power threshold, $P_o > P_{c\_opt}$, the engine remains off. When the power demand exceeds this threshold, the engine is turned on, and the motor provides power assist according to the control parameters shown in Fig. 6. The difference between the total power demand and the power provided by the engine and the motor represents the drive line loss and the auxiliary power demand.

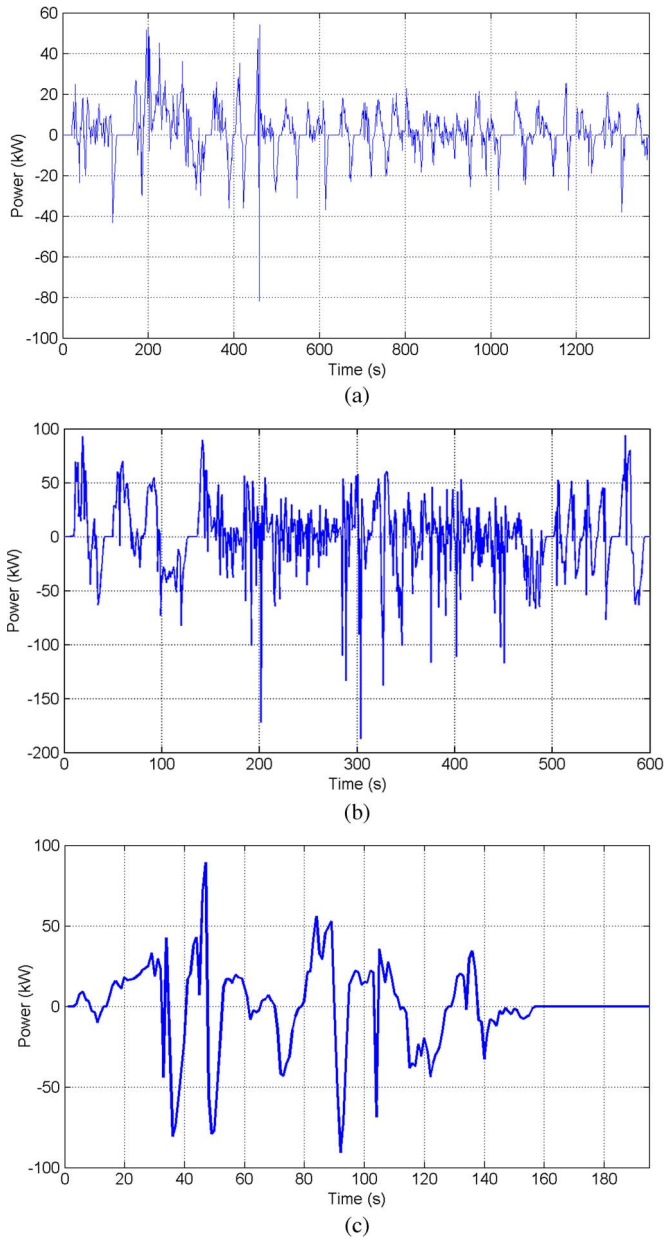

Fig. 10. Total power demand of the different drive cycles. (a). Power demand in the UDDS drive cycle. (b). Power demand in the US06 drive cycle. (c). Power demand in the CR-City drive cycle.

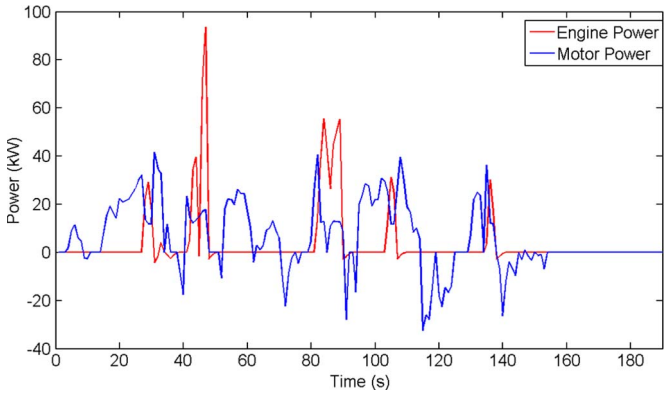

Fig. 11. Power distribution between engine and motor for the CR-City drive cycle.

Figs. 12 and 13 show the power distribution between the engine and the motor for the UDDS and US06 drive cycles. It is shown that, because the power demand in the UDDS drive cycle is relatively low, the engine turn-on time is much less than in the CR-City and US06 drive cycles. It can also be observed in Figs. 11–13 that only a portion of the negative power is recovered by the motor through regenerative braking. This case is consistent with the general practice in HEV control, in which frictional brakes are used to ensure vehicle stability and safety. It can also be observed in Figs. 10–13 that the summation of motor and engine power from is more than the total power demand, because the motor and engine power has to overcome the drive loss and supply power to the auxiliary power demand, which is not included in the vehicle power demand shown in Fig. 10.

In blended-mode PHEVs, the motor power is not sufficient to realize the AER control strategy in high-power demands. The engine provides most of the driving torque in M2, which is obviously not beneficial for fuel economy. Therefore, only M1 was used for simulation and calculation. The simulation results of the PHEV in different drive cycles are shown in Tables VI, which contains the value of fuel mass after SOC correction for the corresponding drive cycles. To compare the fuel consumption results with various strategies, the fuel consumption obtained with M1 is taken as the baseline. It is shown that M3 improves by 4.0%, 4.2%, and 2.56% in 5UDDS, CR-City, and 5US06, respectively.

The fuel savings shown in Table VI obtained by the proposed M3 is primarily due to the reduction in electric system loss. As discussed earlier, the electric system loss significantly increases as the power increases. Hence, there is a threshold at which it is beneficial to turn on the engine to provide the main power for the propulsion power demand while using the motor to supplement the power demand. However, it is important to ensure that the available battery energy is consumed at the end of the drive cycle; otherwise, the battery is underutilized.

To evaluate the fuel economy in the same battery parameters with different CD ranges, different consecutive UDDS drive cycles were adopted. As shown in Fig. 14, the proposed control strategy also achieves better fuel economy than the electric-dominant control strategy, even if the range is greater than 40 mi, but the percent improvement is reduced.

In real-world driving, the trip distance and energy consumption are not precisely known. Modern vehicular navigation systems may provide trip information to be used by the CD strategies. Because the proposed strategy requires only the trip distance and the AER (or the battery energy content), it seems feasible to implement this control strategy for real vehicle applications using the estimated trip information.

VI. Conclusion

A control strategy has been developed based on optimal power operations of the PHEV analyzed from constant vehicle speed operations. A middle-size plug-in SUV model was built in PSAT, and three typical cycles were used to evaluate the fuel consumption. If the trip distance is shorter than the AER and the power demand is low, the AER is the best

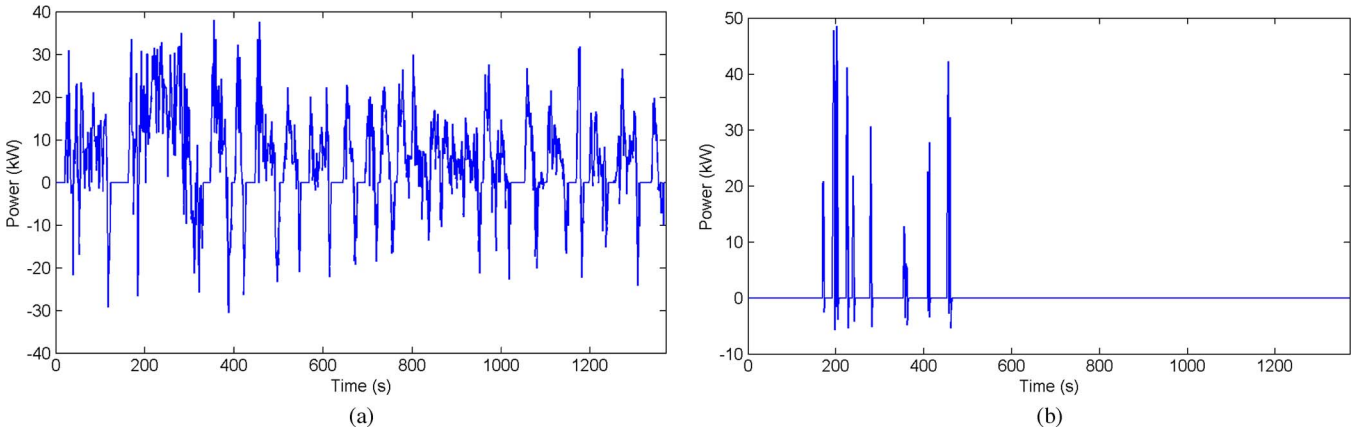

Fig. 12. Power distribution between engine and motor for the UDDS drive cycle. (a). Motor power. (b). Engine power.

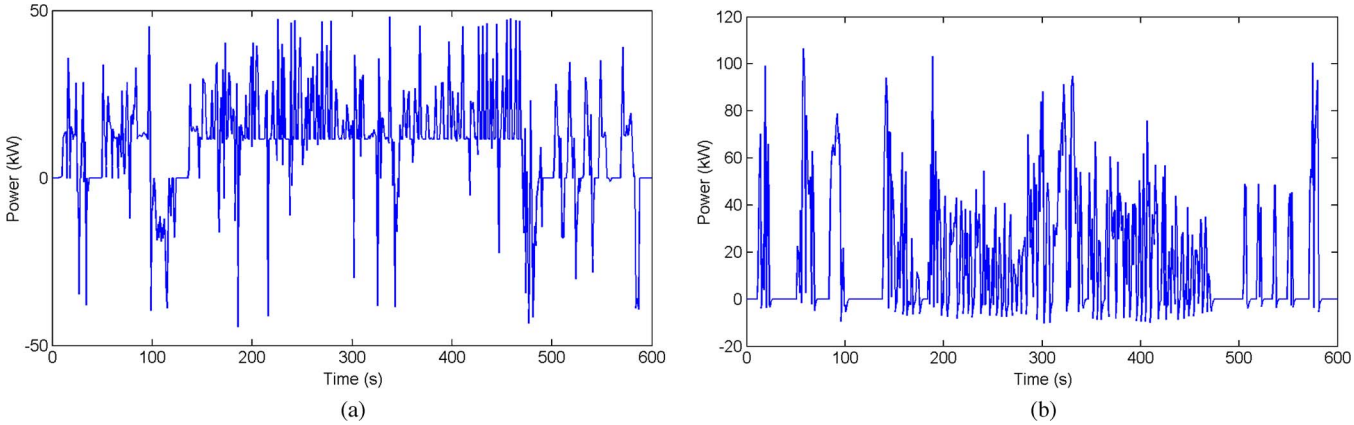

Fig. 13. Power distribution between engine and motor for the US06 drive cycle. (a) Motor power. (b) Engine power.

TABLE VI
TYPICAL DRIVE CYCLE SIMULATION RESULTS

Drive cycle	Fuel consumption (kg) (AED)	Fuel consumption (kg) (Optimal Power)	Fuel savings (%)
5UDDS	2.25	2.16	4.0
CR city	5.72	5.48	4.2
5US06	5.47	5.33	2.56

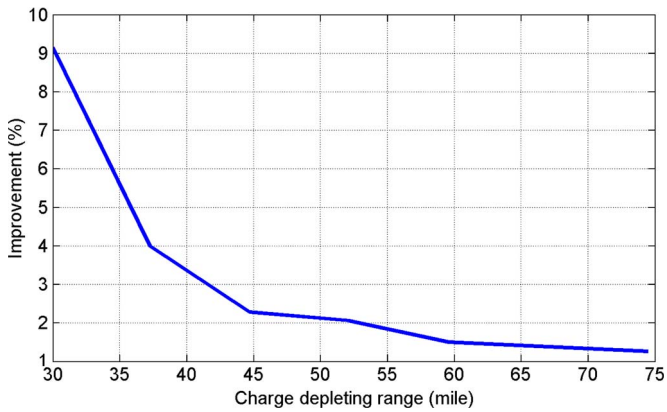

Fig. 14. Improvement with different CD ranges in UDDS.

control strategy. If the drive cycle is more aggressive, the AER will not meet the requirement of high power demand. If the trip distance exceeds the AER, the proposed control strategy M3 can perform better than the electric-dominant control strategy.

In this paper, we only consider the total fuel consumption during specific drive cycles based on the electric system loss characteristics, vehicle power demand, total battery energy, and trip distance. It does not rely on the detailed trip information other than the total trip distance. Therefore, it is possible to implement the control strategy in real time if the total distance is known before the trip. Because most people who commute to work know their approximate driving distance, this control strategy can potentially provide significant fuel savings.

In this paper, only fuel usage has been considered the optimization objective. It is possible to calculate the total energy consumption, which includes fuel and electricity. Hence, the proposed analytical approach can also be used to minimize total energy consumption for given drive cycles. This case will further be explored in future studies.

REFERENCES

[1] A. Simpson, "Cost-benefit analysis of plug-in hybrid electric vehicle technology," presented at the 22nd Int. Battery, Hybrid Fuel Cell Electric Vehicle Symp. Exh., Yokohama, Japan, Oct. 23–28, 2006.

[2] S. S. Williamson, "Electric drive train efficiency analysis based on varied energy storage system usage for plug-in hybrid electric vehicle application," in *Proc. IEEE Power Electron. Spec. Conf.*, Jun. 17–21, 2007, pp. 1515–1520.

[3] V. Freyermuth, E. Fallas, and A. Rousseau, "Comparison of powertrain configuration for plug-in HEVs from a fuel economy perspective," presented at the SAE World Congr. Exh., Detroit, MI, 2008, Paper SAE 2008-01-0461.

[4] Q. Gong, Y. Li, and Z.-R. Peng, "Trip-based optimal power management of plug-in hybrid electric vehicles," *IEEE Trans. Veh. Technol.*, vol. 57, no. 6, pp. 3393–3401, Nov. 2008.

[5] Q. Gong, Y. Li, and Z.-R. Peng, "Trip-based optimal power management of plug-in hybrid electric vehicle with advanced traffic modeling," presented at the SAE World Congr. Exh., Detroit, MI, 2008, Paper SAE 2008-01-1316.

[6] H. Zhao and B. Zhang, "Research on parameters matching of parallel hybrid electric vehicle powertrain," in *Proc. IEEE VPPC*, Sep. 3–5, 2008, pp. 1–4.

[7] F. U. Syed, M. L. Kuang, J. Czubay, and H. Ying, "Derivation and experimental validation of a power-split hybrid electric vehicle model," *IEEE Trans. Veh. Technol.*, vol. 55, no. 6, pp. 1731–1747, Nov. 2006.

[8] J. Liu and H. Peng, "Modeling and control of a power-split hybrid vehicle," *IEEE Trans. Control Syst. Technol.*, vol. 16, no. 6, pp. 1242–1251, Nov. 2008.

[9] J. Meisel, "An analytic foundation for the two-mode hybrid-electric powertrain with a comparison to the single-mode Toyota Prius THS-II," presented at the SAE World Congr. Exh., Detroit, MI, 2009, Paper SAE 2009-01-1321.

[10] T. Katrašnik, "Hybridization of powertrain and downsizing of IC engine: A way to reduce fuel consumption and pollutant emissions—Part 1," *Energy Convers. Manage.*, vol. 48, no. 5, pp. 1411–1423, May 2007.

[11] T. Katrašnik, F. Trenc, and S. R. Opresnik, "Analysis of energy conversion efficiency in parallel and series hybrid powertrains," *IEEE Trans. Veh. Technol.*, vol. 56, no. 6, pp. 3649–3659, Nov. 2007.

[12] J. Gonder and T. Markel, "Energy management strategies for plug-in hybrid electric vehicles," presented at the SAE World Congr. Exh., Detroit, MI, 2007, Paper SAE 2007-01-0290.

[13] P. B. Sharer and A. Rousseau, "Plug-in hybrid electric vehicle control strategy: Comparison between EV and charge-depleting options," presented at the SAE World Congr. Exh., Detroit, MI, 2008, Paper SAE 2008-01-0460.

[14] B. K. Powell, K. E. Bailey, and S. R. Cikanek, "Dynamic modeling and control of hybrid electric vehicle powertrain systems," *IEEE Control Syst. Mag.*, vol. 18, no. 5, pp. 17–33, Oct. 1998.

[15] M. Ehsani, Y. Gao, and K. L. Butler, "Application of electrically peaking hybrid (ELPH) propulsion system to a full-size passenger car with simulated design verification," *IEEE Trans. Veh. Technol.*, vol. 48, no. 6, pp. 1779–1787, Nov. 1999.

[16] C. C. Lin, H. Peng, and J. W. Grizzle, "A stochastic control strategy for hybrid electric vehicles," in *Proc. Amer. Control Conf.*, Boston, MA, Jun. 30–Jul. 2, 2004, pp. 4710–4715.

[17] E. D. Tate, Jr., J. W. Grizzle, and H. Peng, "Shortest path stochastic control for hybrid electric vehicles," *Int. J. Robust Nonlinear Control*, vol. 18, no. 14, pp. 1409–1429, Sep. 2008.

[18] N. N. Clark, W. Xie, M. Gautam, and D. W. Lyons, "Hybrid diesel-electric heavy duty bus emissions: Benefits of regeneration and need for state of charge correction," presented at the Int. Fuels Lubricants Meeting Expo., Baltimore, MD, 2000, Paper SAE-01-2955.

[19] D. L. McKain, N. N. Clark, T. H. Balon, and P. J. Moynihan, "Characterization of emissions from hybrid electric and conventional transit buses," presented at the CEC/SAE Spring Fuels Lubricants Meeting Expo., Paris, France, 2000, Paper SAE 2000-01-2011.

Bingzhan Zhang received the B.S. degree in automotive engineering in 2004 from Hefei University of Technology, Hefei, China, where he is currently working toward the Ph.D. degree with the School of Mechanical and Automotive Engineering.

From September 2008 to August 2010, he was a Visiting Scholar with the DTE Power Electronics Laboratory, Department of Electrical and Computer Engineering, University of Michigan, Dearborn. His research interests include hybrid electric vehicle modeling and supervisory control.

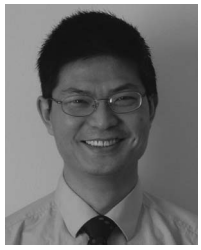

Chris Chunting Mi (SM'00–A'01–M'01–SM'03) received the B.S.E.E. and M.S.E.E. degrees in electrical engineering from the Northwestern Polytechnical University, Xi'an, China, and the Ph.D. degree from the University of Toronto, Toronto, ON, Canada.

He was an Electrical Engineer with General Electric Canada, Inc. He is currently an Associate Professor of electrical and computer engineering and the Director of the DTE Power Electronics Laboratory, Department of Electrical and Computer Engineering, University of Michigan, Dearborn. He has been a Guest Editor of the *International Journal of Power Electronics*, a Member of the Editorial Board of the *International Journal of Electric and Hybrid Vehicles* and the *IET Electrical Systems in Transportation*, and the Associate Editor for the *Journal of Circuits, Systems, and Computers* (2007–2009). He has conducted extensive research and published more than 100 articles. His research interests include electric drives, power electronics, electric machines, renewable energy systems, and electrical and hybrid vehicles.

Dr. Mi received the National Innovation Award, the Government Special Allowance Award, the Distinguished Teaching Award, and the Distinguished Research Award from the University of Michigan, Dearborn. He also received the 2007 IEEE Region 4 Outstanding Engineer Award, the IEEE Southeastern Michigan Section Outstanding Professional Award, and the SAE Environmental Excellence in Transportation Award. From 2008 to 2009, he was the Chair of the IEEE Southeastern Michigan Section. He was the Vice Chair of the IEEE Southeastern Michigan Section from 2006 to 2007 and the Chair in 2008. He was the General Chair of the Fifth IEEE Vehicle Power and Propulsion Conference held in Dearborn on September 6–11, 2009. He is an Associate Editor of the IEEE TRANSACTIONS ON VEHICULAR TECHNOLOGY, an Associate Editor of the IEEE POWER ELECTRONICS LETTERS, and a Senior Editor of *IEEE Vehicular Technology Magazine*.

Mengyang Zhang (M'08) received the M.S. degree in physics from West Virginia University, Morgantown, in 1993.

He is currently a Senior Technical Specialist with the Chrysler Group LLC, Auburn Hills, MI. His research interests include powertrain controls and calibrations for Chrysler hybrid electric vehicle programs and advanced vehicle electrification technologies. He has more than 16 years in the research and development of automotive products, including advanced powertrain, electric drive systems, and chassis systems. He taught a short course on the fundamentals of hybrid electric vehicle powertrains for the IEEE Vehicular Technology Society in 2010.